Published in final edited form as:
Biomaterials. 2008 December ; 29(36): 4847–4854. doi:10.1016/j.biomaterials.2008.08.019.

A Comparison of Fatigue Crack Growth in Human Enamel and Hydroxyapatite

Devendra Bajaj[1], **Ahmad Nazari**[1], **Naomi Eidelman**[2], and **Dwayne Arola**[1,3,♠]

1*Department of Mechanical Engineering, University of Maryland Baltimore County, Baltimore, MD 21250*

2*Paffenbarger Research Center, American Dental Association Foundation, National Institutes of Standards and Technology, Gaithersburg, MD 20899*

3*Department of Endodontics, Prosthodontics, and Operative Dentistry, Baltimore College of Dental Surgery, University of Maryland, Baltimore, MD 21201*

Abstract

Cracks and craze lines are often observed in the enamel of human teeth, but they rarely cause tooth fracture. The present study evaluates fatigue crack growth in human enamel, and compares that to the fatigue response of sintered hydroxyapatite (HAp) with similar crystallinity, chemistry and density. Miniature inset compact tension (CT) specimens were prepared that embodied a small piece of enamel (N=8) or HAp (N=6). The specimens were subjected to mode I cyclic loads and the steady state crack growth responses were modeled using the Paris Law. Results showed that the fatigue crack growth exponent (m) for enamel (m = 7.7±1.0) was similar to that for HAp (m = 7.9±1.4), whereas the crack growth coefficient (C) for enamel (C=8.7E-04 (mm/cycle)·(MPa·$m^{0.5}$)$^{-m}$) was significantly lower ($p<0.0001$) than that for HAp (C = 2.0E+00 (mm/cycle)·(MPa·$m^{0.5}$)$^{-m}$). Micrographs of the fracture surfaces showed that crack growth in the enamel occurred primarily along the prism boundaries. In regions of decussation, the microstructure promoted microcracking, crack bridging, crack deflection and crack bifurcation. Working in concert, these mechanisms increased the crack growth resistance and resulted in a sensitivity to crack growth (m) similar to bone and lower than that of human dentin. These mechanisms of toughening were not observed in the crack growth response of the sintered HAp. While enamel is the most highly mineralized tissue of the human body, the microstructural arrangement of the prisms promotes exceptional resistance to crack growth.

Keywords

decussation; enamel; fatigue; hydroxyapatite; toughening mechanisms

♠Corresponding Author, Dwayne D. Arola, Ph.D., Department of Mechanical Engineering, University of Maryland Baltimore County, 1000 Hilltop Circle, Baltimore, MD 21250 USA, darola@umbc.edu, (410) 455-3310 (v), (410) 455-1052 (f)

INTRODUCTION

Human enamel is regarded as the most highly calcified and hardest tissue of the body. It consists of 96% mineralized material (by weight), with the remaining 4% comprised of an organic matrix and bound water [1]. The microstructure of enamel is comprised of an intricate array of densely packed nanocrystalline carbonated hydroxyapatite arranged within a 'prismshaped' rod structure (4-8 μm in diameter) with organic matter occupying the interprismatic space. The enamel rods extend nominally perpendicular to the dentin enamel junction (DEJ) and increase in effective diameter from the DEJ to the outer surface [2].

Based on its interesting structure and the functional demands it must endure, the mechanical properties of enamel have been examined for many decades. Indentation based studies on enamel have reported a hardness of 3 GPa to 5 GPa [3-5] and an elastic modulus of 70 GPa to 100 GPa [3-7]. These two properties are location dependent, with the occlusal surface exhibiting the highest hardness and elastic modulus [3,7,8]. Due to the limited size available for specimen preparation, indentation based studies have also been used for evaluating the fracture toughness, with reported measures ranging roughly from 0.6 $MPa \cdot m^{0.5}$ to 1.5 $MPa \cdot m^{0.5}$ [3,9-11]. Some of this variation in toughness is associated with the prism orientation; enamel is weakest for crack growth parallel to the rods. When compared with geological hydroxyapatite, enamel is approximately three times tougher [10].

Overall, enamel appears to have a surprisingly low resistance to the initiation and growth of cracks [12]. Indeed, small cracks and craze lines are commonly seen on the outer surface of teeth that are generated due to occlusal forces, temperature variations and restorative processes [13,14]. While these small cracks may not result in tooth fracture, over prolonged periods their growth can be detrimental as they may serve as sites for demineralization [15], and further mechanical degradation. Thus, the conditions associated with crack initiation in enamel and the process of cyclic crack extension is of both scientific and clinical interest. However, to the authors' knowledge there has been no reported evaluation that quantifies the fatigue and fatigue crack growth properties of enamel. As such, the mechanisms contributing to the crack growth resistance of this tissue have remained unknown.

The primary objectives of this study were to quantify cyclic crack growth in human enamel, and to develop a mechanistic understanding of crack extension in this tissue. To assess the role of microstructure, the crack growth resistance of enamel was compared with that of a sintered HAp with similar density and chemical composition. The results provide the first quantitative description for the fatigue properties of enamel.

MATERIALS AND METHODS

Caries-free third molars extracted from patients 17 years to 27 years old were acquired from participating dental practices in Maryland according to an approved protocol by the Institutional Review Board of the University of Maryland Baltimore County. Sections of enamel ($2\times2\times2$ mm^3) were obtained from the cuspal region using diamond impregnated slicing equipment (K.O. Lee Model S3818EL, Aberdeen, SD, USA) under continuous hydration (Fig. 1(a)). All enamel specimens were prepared with the prisms oriented parallel to the expected plane of crack growth, which is the orientation with lowest toughness [10] and consistent with the crack growth direction *in vivo*. Specimens were obtained from the sintered HAp pellets (2mm thick and 6mm diameter, density: 2.99 g/cm^3, Clarkson Chromatography Products Inc, Williamsport, PA) using the same approach. For comparison, the density of enamel is roughly 3.02 g/cm^3 [16].

Prior to an evaluation of mechanical behavior, the chemical composition of the enamel and HAp were characterized. For chemical analysis of the enamel, particles were retrieved from

near the occlusal surface of a dry tooth with a dental bur and subsequently ground to a fine powder. The HAp pellets (i.e. the control) were selected for examination as they exhibited similar crystal structure and chemical composition to the enamel, but much simpler microstructure. One pellet of the HAp was crushed and ground to a fine powder using a mortar and pestle. A fine powder of highly crystallized stoichiometric hydroxyapatite* was used as reference standard for comparison to the commercial sintered Hap pellets. This material was prepared in solid state reactions at 900 °C to 1100 °C and its chemical composition was fully determined in an earlier investigation [17]. The HAp and enamel powders, as well as that of the highly crystallized hydroxyapatite (OHAp), were subjected to x-ray diffraction (XRD) analysis. The XRD patterns were recorded in the 2θ range from 4° to 65° in intervals of 0.010° 2θ with CuKα radiation (λ = 0.154 nm) using a Rigaku 2200 D-Max X-ray diffractometer (Rigaku/USA Inc., Danvers, MA, USA) operating at 40 kV and 40 mA.

Small amounts of the same powders that were subjected to XRD (0.22 mg to 0.25 mg) were embedded in 400 mg of spectroscopic grade potassium bromide and pressed into pellets (13 mm diameter, 1 mm thick). Spectra were collected from the pellets using Fourier Transform Infrared (FTIR) spectroscopy from 4000 cm^{-1} to 400 cm^{-1} at a resolution of 2 cm^{-1} with 256 co-added scans using a Nicolet Nexus 670 FTIR spectrophotometer (Nicolet Instrumentations Inc. Madison, WI, USA) continuously purged with dry air. The peak locations and intensities were determined with the Omnic software (Nicolet Instrumentations Inc. Madison, WI, USA). The relative intensity was calculated by dividing the intensity of each peak by the intensity of the highest peak in the spectrum (the ψ_3PO_4 at ~ 1046cm^{-1} in all three spectra). The main bands at the ψ_3PO_4 domain (1225 cm^{-1} to 900 cm^{-1}) and at the ψ_4PO_4 domain (675 cm^{-1} to 495 cm^{-1}) spectral regions were separated with PeakFit™ (Jandel corporation, San Rafael, CA, USA) using linear baseline and Lorentz peak area function. The resolved peaks center and width at half the height (FWHM) were determined.

To enable fatigue crack growth testing the enamel and HAp sections were molded within a specimen comprised of Vit-l-escence (Ultradent Products, Inc., South Jordan, UT, USA) resin composite with overall dimensions of 8×6×2 mm^3 (Fig. 1(b)). Bonding of the enamel and HAp sections to the resin composite was achieved using a total etch adhesive resin system (Optibond solo plus, Kerr Corporation, Orange, CA, USA). The inset placement was optimized according to a finite element model to balance concerns associated with interfacial stresses and stress intensity distribution. Detailed descriptions of bonding procedures and numerical methods are given elsewhere [18, 19]. After molding, the inset CT specimens were lightly sanded (up to 4000-grit finish) with subsequent polishing using diamond particle suspension of sizes 9, 3 and 0.04 μm (Buehler) with a standard cloth wheel. A channel (1 mm wide) was introduced on the back of all specimens to guide the direction of crack extension. Two holes were counter-bored for application of the opening mode loads as shown in Figure 1(b). Lastly, a chevron notch was machined using a diamond impregnated slicing wheel and the tip was sharpened using a razor blade and diamond paste (1 μm particles) to facilitate crack initiation.

All specimens were subjected to cyclic loading using an Enduratec Model ELF 3100 universal testing system. The enamel specimens were tested within a hydration bath of Hanks Balanced Salt Solution (HBSS) at 22°C while the HAp specimens were tested in ambient air to minimize the potential for dissolution. Crack initiation in all specimens was achieved using a cyclic stress ratio (R) of 0.1, frequency of 5 Hz and maximum load between 3 to 5 Newtons for enamel and between 1 and 2 Newtons for HAp. Cyclic loading of the specimens after crack initiation (crack length ~ 0.4 mm) was continued under R=0.1 and frequency of 5 Hz until fracture. Measurements of crack extension (Δa) over selected increments of growth (ΔN) were (obtained using a digital microscope (Navitar, IEEE 1394) at a magnification of 30X. The incremental

*Donated by Mr. B. O. Fowler (formerly with the National Institute of Dental and Craniofacial Research, NIH).

measurements were used in quantifying the fatigue crack growth rate (da/dN). Additional details of the fatigue loading and method of crack length measurement have been described elsewhere [20].

The steady state portion (Region II) of the fatigue crack growth response (Fig. 1(c)) was quantified using the Paris Law [21] according to

$$\frac{da}{dN}=C(\Delta K)^m \quad (1)$$

where ΔK is the stress intensity range, and m and C are the fatigue crack growth exponent and coefficient, respectively. The ΔK for the inset specimens was estimated using results of a numerical model for crack extension in terms of the specimen geometry and cyclic load according to

$$\Delta K=\frac{\Delta P}{B\sqrt{W}}\left(0.87-3.97\alpha+7.04\alpha^2\right) \quad (2)$$

where ΔP (P_{max}-P_{min}) is the cyclic load range, α is the ratio of a to W, and B is the ligament thickness (Fig. 1(b)). The quantities m and C were obtained from the slope of the steady state (Region II) crack growth response and the intercept, respectively (Fig. 1(c)). The average coefficient (C) was estimated from the antilog of the average of log(C). In addition, a pooled response was determined for each material where all growth data was combined to form a single response. This treatment assumes that the material for all specimens is the same (as is typical for an engineering material). The cumulative experimental responses obtained for each group of specimens were used in estimating the mean and standard deviation for all the properties of interest. Outliers within the groups of m and C obtained for each material were identified using the Grubbs test and discarded. Then, statistical differences between the two groups were evaluated using the student's t test and were considered to be significant at $p<0.05$. Fracture surfaces were evaluated using a scanning electron microscope (SEM, model JSM 5600, JEOL Inc., Peabody, MA) in secondary electron imaging mode.

RESULTS

The XRD patterns of the enamel, HAp and OHAp are presented in Figure 2(a). Patterns from the HAp and enamel are almost identical to that of the OHAp and contain all the OHAp reflections over the range of evaluation. Note that the 2θ range from 37 ° to 65 ° is not shown. There are four additional very small peaks in the ground HAp at 2θ of 4.66 °, 11.6 °, 11.6 °, 33.6 ° (Fig. 2(a)) and 42.9 ° (not shown) that did not match reflections of calcium oxide, calcium hydroxide or any of all known calcium phosphate compounds. Nevertheless, the relative difference in the crystal structure between the HAp and enamel is very small. The FTIR spectra of the enamel, HAp and OHAp are shown in Figure 2(b). Comparison between the spectra of enamel and HAp and the position and relative intensity of the main peaks, and the centers and widths of the resolved peaks reveals that the enamel's frequencies shift towards lower values in six out of the seven examined peaks (0.1 to 6.5 cm^{-1}) and resolved peaks (1.3 to 8.4 cm^{-1}). Only the ψ_4PO_4 at about 603 cm^{-1} shifted to higher frequency. The relative intensity and the widths of the resolved peaks of the enamel were slightly higher and larger in five of the six examined peaks (2.9 to 6.2% and 0.8 to 12.3 cm^{-1}, respectively). All the PO_4 and OH peaks of both the enamel and HAp are present at about the same location in the OHAp spectrum, but those of the HAp are closer to the frequency of the OHAp than of enamel. Note also that the peaks are narrower and of higher relative intensity in the OHAp, which is indicative of higher crystallinity. There is one additional peak in the spectrum of the HAp at 435 cm^{-1} that is not represented in the enamel or OHAp. This peak is originated from oxide translation of partially dehydroxylated hydroxyapatite caused by the thermal treatment [22]. According to both XRD and FTIR analyses, the crystal structure and chemical composition of the enamel and HAp are

close, except for the presence of carbonate (CO_3) in enamel. Carbonate absorptions are seen in the enamel spectrum at the 1350 cm^{-1} to 1590 cm^{-1} spectral region and at 873 cm^{-1}; it appears that both type B (PO_4 replacement) and type A (OH replacement) are present. The absorption at 878 cm^{-1} (appears as a small split from 873 cm^{-1} carbonate peak) originates from HPO_4.

The steady state fatigue crack growth responses for the enamel and sintered HAp are shown in Figure 3. Overall, the steady state crack growth rates for both groups ranged approximately from 10^{-6} mm/cycle to 10^{-3} mm/cycle. Region II cyclic extension in enamel occurred over a stress intensity range from 0.35 MPa·$m^{0.5}$ to 0.80 MPa·$m^{0.5}$, whereas in HAp it occurred over a ΔK from 0.15 MPa·$m^{0.5}$ to 0.30 MPa·$m^{0.5}$. An extrapolation of the Region II responses (Fig. 1(c)) was used to obtain a first order estimate of the stress intensity threshold (ΔK_{th})[†]. The estimated ΔK_{th} for enamel (~0.35 MPa·$m^{0.5}$) was approximately three times that of the HAp (~0.13 MPa·$m^{0.5}$). Paris Law parameters for the enamel and HAp are listed in Table 1 and Table 2, respectively. The average Paris Law exponent for enamel (m = 7.7±1.0) was similar to that of the HAp (m = 7.9±1.4). However, the average crack growth coefficient for HAp (C = 2.0E+00 (mm/cycle)·(MPa·$m^{0.5}$)$^{-m}$) was significantly higher ($p<0.0001$) than that for enamel (C = 8.7E-04 (mm/cycle)·(MPa·$m^{0.5}$)$^{-m}$). In addition, the pooled response for enamel resulted in m=3.9 and C = 1.0E-04 (mm/cycle)·(MPa·$m^{0.5}$)$^{-m}$ whereas for the HAp m = 7.6 and C =9.0E +00 (mm/cycle)·(MPa·$m^{0.5}$)$^{-m}$. Results of both assessments distinguish the higher crack growth resistance of enamel in comparison to the HAp.

The crack path and fracture surface characteristics revealed that there were distinct differences in the nature of crack extension between the enamel and the HAp. An optical micrograph that documents extension in an enamel specimen is shown in Figure 4(a). Note that the crack path is not continuous and that the crack surfaces are spanned by a large number of unbroken ligaments of tissue tens to hundreds of a micrometer long. There was also evidence of sharp crack deflection and crack bifurcation during growth in the steady state region, which appears to result from a change in the prism orientation within regions of acute decussation. Images of the fractured surfaces revealed that the cracks extended primarily along the prisms in enamel. As such, the plane of fracture was not flat, but exhibited a “waviness” that increased in amplitude with growth from the point of initiation (outer enamel) towards the DEJ (Fig. 4(b)). Further evaluation of the fracture surfaces at higher magnification showed that a series of several small ligaments (Fig. 4(c)) developed that were from one to five prisms in thickness. At even higher magnification there was additional complexity in the fracture surface (Fig. 4 (d)). Within regions of decussation, crack extension induced fracture oblique to the prism axis and was accompanied by the development of ligaments comprised of nano crystalline rods as highlighted in Figure 4(d). Fracture of the prisms occurred in a tortuous manner as evident from the large surface roughness. In contrast to these features, the crack path in the HAp was straight and showed no evidence of bridging. The fracture surfaces of the HAp specimens appeared comparatively smooth (Fig. 5(a)) despite the presence of a few voids (Fig. 5(b)) and regions of intergranular fracture that extended beneath the nominal fracture plane (Fig. 5(c)).

DISCUSSION

An evaluation of fatigue crack growth in human tooth enamel and a sintered HAp was conducted using a unique inset CT specimen. The primary results of this work show that despite having similar density and chemistry[‡] (Fig. 2), the enamel and HAp exhibited distinctly different fatigue crack growth responses. In comparing crack initiation behavior, the HAp required a substantially lower driving force as the ΔK_{th} for the HAp (~0.13 MPa·$m^{0.5}$) was

[†]The stress intensity threshold (ΔK_{th}) is defined as a critical stress intensity below which fatigue crack growth is presumed not to occur or, occurs at a very slow rate. An ‘apparent’ or ‘first order’ estimate of ΔK_{th} can be obtained by extrapolating the Region II growth response to an appreciably small growth rate (e.g. 10^{-7} mm/cycle).

approximately one third that of enamel (~0.35 MPa·$m^{0.5}$). It is important to highlight that fatigue crack growth in the HAp was conducted dry and the presence of moisture would promote an even lower threshold as the hydroxyl group shows a strong affinity towards water [24]. In contrast, the presence of moisture in enamel is considered important for maintaining structural integrity of the protein matrix, and consequently in regulating the mechanical properties [25, 26]. In addition to differences in the initiation behavior, significant differences were noted between the steady state crack growth responses of the enamel and HAp. The average fatigue crack growth exponent (m) for the enamel was similar to that of the sintered HAp emphasizing equal sensitivity to crack growth and degree of brittleness. However, the average crack growth coefficient (C) for enamel was over three orders of magnitude lower than that for HAp. Steady state crack growth in enamel occurred over a stress intensity range (ΔK) more than three times that of HAp, indicating that (enamel enrolls fracture processes that promote energy absorption and provide superior crack growth resistance. Lastly, using the fatigue crack growth responses to obtain a first order estimate of fracture toughness (K_C)[§] results in a K_C of 0.9 MPa·$m^{0.5}$ for enamel. This value agrees well with the range reported in the literature (0.6 -1.5) MPa·$m^{0.5}$ which to date has been obtained exclusively using indentation techniques [3,9,11]. The K_C estimate for enamel is three times higher than that of the HAp (~0.3 MPa·$m^{0.5}$).

The values of m and C obtained in this study are the first reported measures of the Paris Law parameters for enamel and HAp. Caution must be exercised in interpreting the quantitative measure of fatigue crack growth parameters in enamel as the apparent stress intensity at the crack tip should be corrected for the presence of crack bifurcation and crack deflection (Fig. 4(a)). Such corrections are beyond the scope of this study. Although it is not possible to compare these results with previous studies on enamel a comparison to fatigue crack growth responses reported for human bone [28] and human dentin [20] is shown in Figure 6(a). It should be noted that due to the differences in microstructure and organic content, the fatigue processes responsible for cyclic crack extension in the enamel, and certainly the HAp, may be quite different than those in dentin and bone. As such, the quantitative comparison of the growth responses in Figure 6(a) highlights the differences in rate, but does not imply that the contributing mechanisms are consistent. Overall, the HAp is least resistant to cyclic crack growth, and as expected, the ΔK_{th} for enamel (~0.35 MPa·$m^{0.5}$) is less than that of human dentin (~0.7 MPa·$m^{0.5}$) [20] and human bone (~ 0.45 MPa·$m^{0.5}$ to 0.60 MPa·$m^{0.5}$) [28]. This trend is at least partly attributed to the higher mineral content and crystallinity of enamel to that of bone and dentin (Fig. 6(b)). Steady state crack extension occurs over a similar range of driving force in these three tissues. Surprisingly, enamel is approximately equally sensitive to crack growth as human bone (m ~ 4.4-9.5) [28] and less sensitive to crack growth than human dentin (m = 13.3±1.1) [20]. Due to the large organic content of bone and dentin in comparison to enamel, these results suggest that the microstructure of enamel is extremely effective in promoting crack growth resistance in this hard and brittle material. Indeed, a 4% increase in organic content over that of HAp results in a 3-fold increase in growth toughness.

Cyclic crack extension in bone [28] and dentin [29,30] has been found to occur through a process of crack tip blunting and resharpening, and is accompanied by some interesting

[‡]The HAp contains traces of dehyoxylated hydroxyapatite and an unknown impurity which are not present in enamel. The most distinct difference in the chemical composition of the materials is the presence of carbonate (CO_3) in enamel. There is an increase in CO_3 from outer to inner enamel, resulting in a decrease in crystallinity towards the DEJ [23]. Nevertheless, the influence of carbonate related changes on mechanical properties of enamel are still unclear.

[§]A materials resistance to failure under montonic, quasi-static loading conditions is characterized by a critical value of the stress intensity factor and is termed the fracture toughness K_C. For low values of stress ratio (R) the maximum stress intensity factor (K_{max}) with a fatigue cycle approaches the fracture toughness of the material within Region III [27]

$$K_{max} = \frac{\Delta K}{1 - R} \approx K_C$$

mechanisms of crack growth resistance. Both dentin and bone enroll a combination of near-tip microcracking and crack bridging by unbroken ligaments that form in the crack wake. A distinction of whether the documented crack extension in enamel occurred through “true” fatigue (i.e. cyclic processes) or primarily under the static component of the cycle (i.e. the means stress) was not distinguished. Due to the comparatively low organic content of enamel it is not clear whether there are near-tip inelastic processes that contribute to the growth cycle. Those aspects of extension were certainly not active in the Hap. However, cyclic crack extension in the enamel was found to be accompanied by crack bifurcation, sharp crack deflections and unbroken ligaments (~30-100 μm in length) of tissue that bridge the crack (Fig. 4(a)) and promote crack growth resistance via closure forces; the unbroken ligaments were most evident in the inner enamel. The number of unbroken ligaments that formed over a millimeter of crack growth appeared to be far greater in enamel than that reported in studies of either bone [28] or dentin [29]. Again, these components of toughening were not active during crack extension within the Hap, which is one of the primary factors responsible for the differences in the growth responses.

An evaluation of the fracture surface revealed that crack growth in enamel occurred parallel to the long axis of the prisms and was mostly confined to the interprismatic enamel (Fig. 4(c)). However, there was a prominent variation in the fracture plane across the thickness that was comprised of multiple crack tilts (Fig. 4(b)). These periodic deflections increase in amplitude and frequency towards the DEJ (Fig. 4(c)) and were caused by the crossing of bundles of prisms (also known as decussation [31]). Such periodic deflections have also been observed in other evaluations of enamel [32]. Crack growth across the decussated enamel also resulted in formation of smaller ligament bridges (~10-30 μm in length) spread across the specimen thickness (Fig. 4(c)). In contrast to these observations, fracture surfaces of the HAp appeared to be relatively flat and smooth with no apparent contributor to energy dissipation or toughening (Fig. 5). Thus, decussation in enamel appears to play the primary role in crack growth resistance. Cracks from the outer enamel are guided within this complex intertwined structure by the interprismatic boundaries, and then are arrested or lose significant energy as a result of a concert of mechanisms. Subsequent growth is achieved when the crack finds a more favorable or less energetic path in the interprismatic boundary of adjacent prisms (Fig. 7).

Cracks that develop and extend in the occlusal enamel are generally arrested at the DEJ. Previous studies have attributed the arrest to the higher toughness of the DEJ [33] and the underlying mantle dentin [34]. Results from the present evaluation suggest that the enamel is an integral contributor to the high apparent toughness of the DEJ. The toughening mechanisms identified herein (summarized in Fig. 7) suggest that like in bone [35] and dentin [36], human enamel exhibits a rising toughness with crack extension. However, while bridging is believed to originate from microcracks in the mineralized phase of the collegeneous tissues [37], the formation of unbroken ligaments in enamel results from microcracks (interprismatic loosening) that develop in and around the organic phase. As such, the organic matrix of the interprismatic space acts as a mechanical guide by offering the least resistant path for crack extension. However, wandering of the crack along the complex mesh of prism bundles results in energy dissipation via friction, pull-out and ultimately fracture of the prisms (Fig. 4(d)). These mechanisms are perhaps even more complicated at the nano-scale (Fig. 4(d)) where crack progression would result in an effective transfer of stress from the stiff mineralized nano-particles to the softer organic material present between adjacent nanocrystals. Further investigation is underway to understand the contribution of these individual micro and nano-scale mechanisms to the toughness of enamel and the apparent toughness of the DEJ. Lastly, the present work did not discern whether the apparent cyclic crack growth response in enamel was due to “true” fatigue, akin to the behavior of bone [28] and dentin [30] or whether the enamel underwent quasi-brittle mechanisms of crack extension. Future work will address this

aspect of mechanical behavior, as well as contributions of the interprismatic proteins on the extension process.

CONCLUSIONS

An evaluation of fatigue crack growth in enamel and sintered HAp was conducted using a special inset CT specimen. From a comparison of the structure, chemistry and the fatigue crack growth responses of these two materials, the following conclusions were drawn:

1. Steady state fatigue crack growth within enamel occurred over a stress intensity range (ΔK) from 0.35 MPa·$m^{0.5}$ to 0.80 MPa·$m^{0.5}$. In the HAp fatigue crack growth occurred over ΔK from 0.15 MPa·$m^{0.5}$ to 0.3 MPa·$m^{0.5}$. The average growth rates for both materials ranged from approximately 1E-06 mm/cycle to 1E-03 mm/cycle. At the driving force (ΔK) the average rate of cyclic crack extension in the HAp was over three same orders of magnitude higher than that in enamel.
2. The enamel (m=7.7±1.0) and HAp (m=7.9±1.4) exhibited similar sensitivity to crack growth. However, the average fatigue crack growth coefficient for enamel (C=8.7E-04 (mm/cycle)·(MPa·$m^{0.5}$)$^{-m}$) was significantly lower ($p<0.0001$) than that for HAp (C=2.0E+00 (mm/cycle)·(MPa·$m^{0.5}$)$^{-m}$).
3. The XRD and FTIR analyses distinguished that there were no significant differences in the chemistry of the HAp and enamel. Thus the higher crack growth resistance of enamel is primarily attributed to the structural arrangement of the prisms and the organic matrix.
4. Fatigue crack growth in enamel occurred primarily parallel to the prisms and along the interprismatic enamel. Several mechanisms of toughening contributed to the crack growth resistance including crack bridging, crack deflection and crack bifurcation. These mechanisms were not observed in the fatigue crack growth response of the HAp. Decussation of the enamel prisms promotes an increase in the resistance to crack extension with proximity to the DEJ.

ACKNOWLEDGEMENTS

This work was supported in part by the NSF (BES0521467) and the NIDCR (DE016904). The authors would like to thank Ultradent Products Inc for supplying the Vit-l-escence resin composite and Dr. Judith Porter of the University of Maryland, Baltimore for bonding supplies. The authors also wish to acknowledge the efforts of Nikhil Amin for technical assistance.

Support for the following investigation was provided by the NSF (BES0521467) and the NIDCR (DE016904)

REFERENCE

1. Ten Cate, AR. Oral histology: Development, structure and function. 4. Mosby; St. Louis: 1994.
2. Robinson, C.; Kirkham, J.; Shore, R. Dental enamel: Formation to destruction. CRC press; Boca Raton: 1995.
3. Xu HHK, Smith DT, Jahanmir S, Romberg E, Kelly JR, Thompson VP, et al. Indentation damage and mechanical properties of human enamel and dentin. J Dent Res 1998;77:472–480. [PubMed: 9496920]
4. Habelitz S, Marshall SJ, Marshall GW Jr, Balooch M. Mechanical properties of human dental enamel on the nanometer scale. Arch Oral Biol 2001;46:173–183. [PubMed: 11163325]
5. Mann AB, Dickinson ME. Nanomechanics, chemistry and structure at the enamel surface. Monogr Oral Sci 2006;19:105–131. [PubMed: 16374031]
6. Balooch G, Marshall GW, Marshall SJ, Warren OL, Asif SA, Balooch M. Evaluation of a new modulus mapping technique to investigate microstructural features of human teeth. J Biomech 2004;37:1223–1232. [PubMed: 15212928]

7. He LH, Fujisawa N, Swain MV. Elastic modulus and stress-strain response of human enamel by nanoindentation. Biomaterials 2006;27:4388–4398. [PubMed: 16644007]
8. Park S, Wang DH, Zhang D, Romberg E, Arola D. Mechancal properties of human enamel as a function of age And location in the tooth. J Mater Sci Mater Med. 2008in press
9. Hassan R, Caputo AA, Bunshah RF. Fracture toughness of human enamel. J Dent Res 1981;60:820–827. [PubMed: 6937518]
10. White SN, Luo W, Paine ML, Fong H, Sarikaya M, Snead ML. Biological organization of hydroxyapatite crystallites into a fibrous continuum toughens and controls anisotropy in human enamel. J Dent Res 2001;80:321–326. [PubMed: 11269723]
11. Park S, Quinn JB, Romberg E, Arola D. On the brittleness of enamel and selected dental materials. Dent Mater. 2008in press
12. Rasmussen ST, Patchin RE. Fracture properties of human enamel in an aqueous environment. J Dent Res 1984;63:1362–1368. [PubMed: 6595288]
13. Abou-Rass M. Crack lines: The precursors of tooth fractures- their diagnosis and treatment. Quintessence Int Dent Dig 1983;14:437–447. [PubMed: 6574554]
14. Xu HH, Kelly JR, Jahanmir S, Thompson VP, Rekow ED. Enamel subsurface damage due to diamond tooth-preparation. J Dent Res 1997;76:1698–1706. [PubMed: 9326903]
15. Walker BN, Makinson OF, Peters MC. Enamel cracks. The role of enamel lamellae in caries initiation. Aust Dent J 1998;43:110–116. [PubMed: 9612985]
16. Wilson RM, Elliott JC, Dowker SEP. Rietveld refinement of the crystallographic structure of human dental enamel apatites. Am Miner 1999;84:1406–1414.
17. Fowler BO. Infrared studies of apatites .2. Preparation of normal and isotopically substituted calcium, strontium, and barium hydroxyapatites and spectra-structure-composition correlations. Inorg Chem 1974;13(1):207–214.
18. Soappman M, Nazari A, Porter JA, Arola D. A comparison of fatigue crack growth in resin composite, dentin and the interface. Dent Mater 2007;23:608–614. [PubMed: 16806452]
19. Zhang D, Nazari A, Soappman M, Bajaj D, Arola D. Methods for examining the fatigue and fracture behavior of hard tissues. Exp Mech 2007;47:325–336.
20. Bajaj D, Sundaram N, Nazari A, Arola D. Age, dehydration and fatigue crack growth in dentin. Biomaterials 2006;27:2507–2517. [PubMed: 16338002]
21. Paris PC, Erdogan F. A critical analysis of crack propagation laws. J Basic Eng 1961;D85:528–534.
22. Kuroda S, Fowler BO. Compositional, structural, and phase-changes in in vitro laser-irradiated human tooth enamel. Calcif Tiss Int 1984;36(4):361–369.
23. LeGeros RZ, Sakae T, Bautista C, Retino M, LeGeros JP. Magnesium and carbonate in enamel and synthetic apatites. Adv Dent Res 1996;10:225–231. [PubMed: 9206341]
24. Benaqqa C, Chevalier J, Saädaoui M, Fantozzi G. Slow crack growth behavior of hydroxyapatite ceramics. Biomaterials 2005;26:6106–6112. [PubMed: 15890401]
25. He LH, Swain MV. Influence of environment on the mechanical behavior of human enamel. Biomaterials 2007;28:4512–4520. [PubMed: 17659336]
26. He LH, Swain MV. Understanding the mechanical behaviour of human enamel from its structural and compositional characteristics. J Mech Behav Biomed Mater 2008;1:18–29.
27. Suresh, S. Fatigue of materials. 2nd ed.. Cambridge University Press; Cambridge: 1998.
28. Nalla RK, Kruzic JJ, Kinney JH, Ritchie RO. Aspects of in vitro fatigue-crack growth in human cortical bone: Time- and cycle-dependent crack growth. Biomaterials 2005;26:2183–2195. [PubMed: 15576194]
29. Bajaj D, Sundaram N, Arola D. An examination of fatigue striations in human dentin: In-vitro and in-vivo. J Biomed Mater Res 2008B;85:149–159.
30. Kruzic JJ, Nalla RK, Kinney JH, Ritchie RO. Mechanistic aspects of in vitro fatigue-crack growth in dentin. Biomaterials 2005;26:1195–1204. [PubMed: 15451639]
31. Skobe Z, Stern S. The pathway of enamel rods at the base of cusps of human teeth. J Dent Res 1980;59:1026–1032. [PubMed: 6929287]

32. Rensberger, JM. Pathway to functional differentiation in mammalian enamel. In: Teaford, MF.; Smith, MM.; Ferguson, MWJ., editors. Development, function and evolution of teeth. Cambridge University Press; 2000.

33. Marshall SJ, Balooch M, Habelitz S, Balooch G, Gallagher R, Marshall GW. The dentin-enamel junction-a natural, multilevel interface. J Eur Ceram Soc 2003;23:2897–2904.

34. Imbeni V, Kruzic JJ, Marshall GW, Marshall SJ, Ritchie RO. The dentin-enamel junction and the fracture of human teeth. Nat Mater 2005;4:229–232. [PubMed: 15711554]

35. Nalla RK, Kruzic JJ, Kinney JH, Ritchie RO. Mechanistic aspects of fracture and R-curve behavior in human cortical bone. Biomaterials 2005;26:217–231. [PubMed: 15207469]

36. Koester KJ, Ager JW III, Ritchie RO. The effect of aging on crack-growth resistance and toughening mechanisms in human dentin. Biomaterials 2008;29:1318–1328. [PubMed: 18164757]

37. Nalla RK, Kruzic JJ, Ritchie RO. On the origin of the toughness of mineralized tissue: microcracking or crack bridging? Bone 2004;34:790–798. [PubMed: 15121010]

(a)

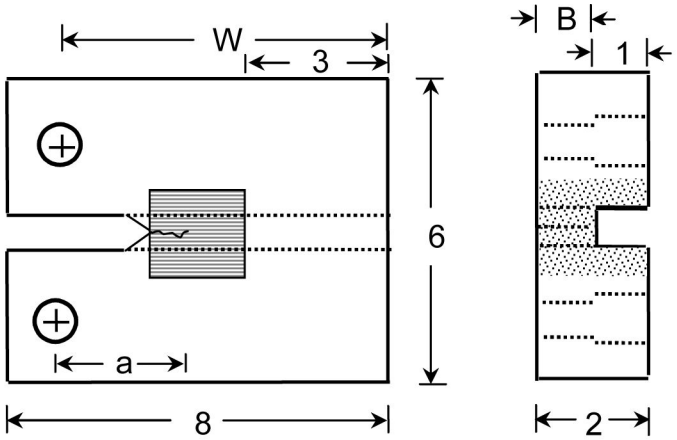

(b)

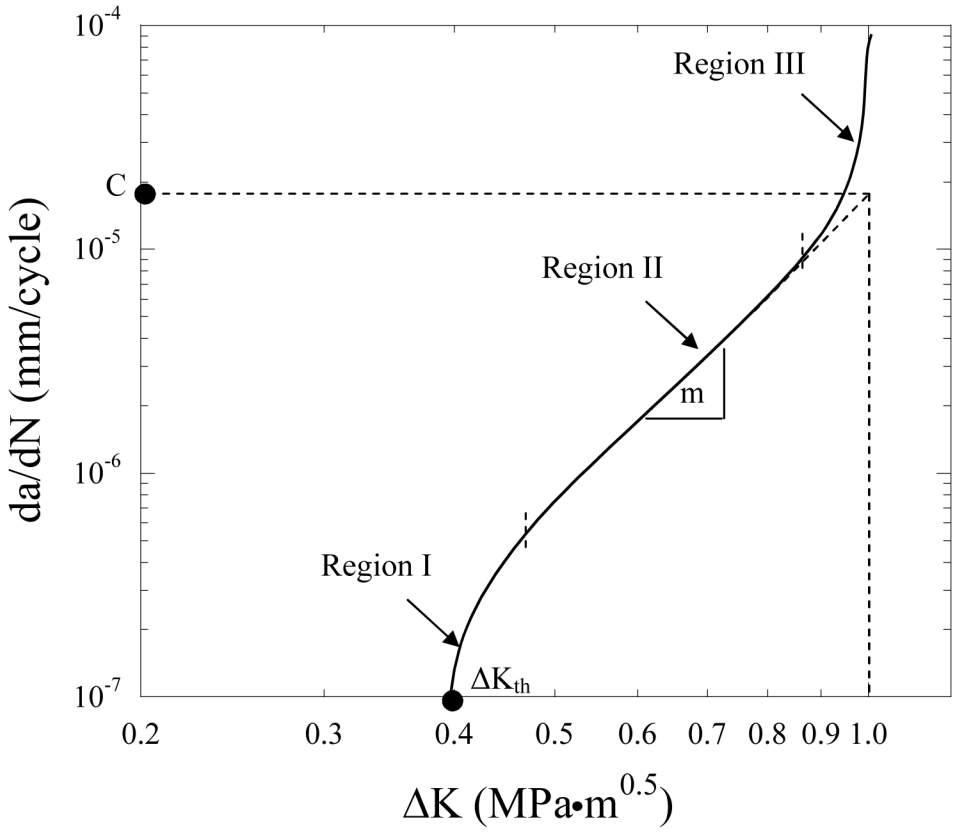

(c)

Figure 1.

Details pertaining to preparation and geometry of the inset compact tension (CT) specimens, and the fatigue crack growth testing of enamel and HAp.

(a) a section of 3rd molar and possible inset enamel, arrow indicates the expected direction of crack growth

(b) final geometry of inset enamel CT specimen (all dimensions in mm). The inset HAp specimen had the same geometry as the inset enamel specimen

(c) a typical fatigue crack growth response distinguishing the three regions of crack extension and the Paris Law parameters

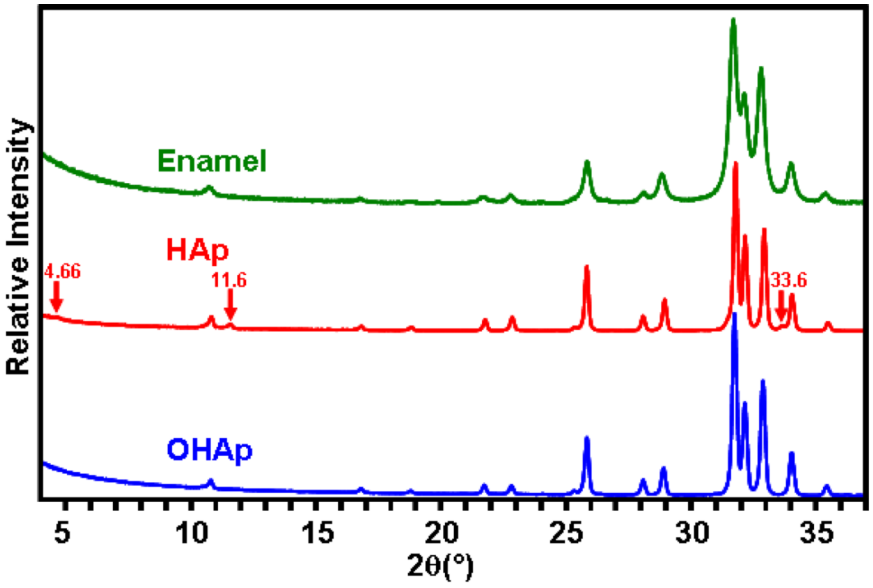

(a)

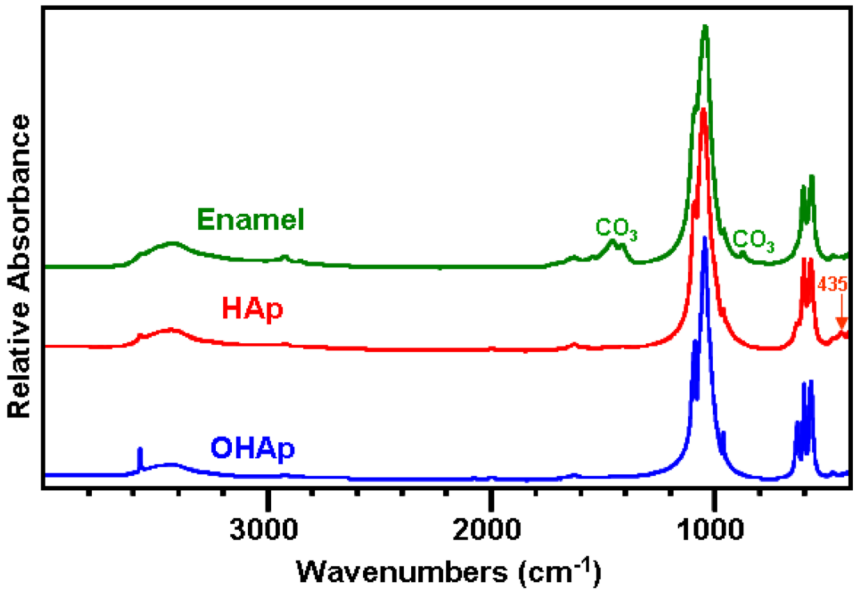

(b)

Figure 2.

XRD patterns (a) and FTIR spectra (b) for human enamel, sintered hydroxyapatite (HAp) and highly crystalline hydroxyapatite (OHAp).

(a) XRD patterns

(b) FTIR patterns

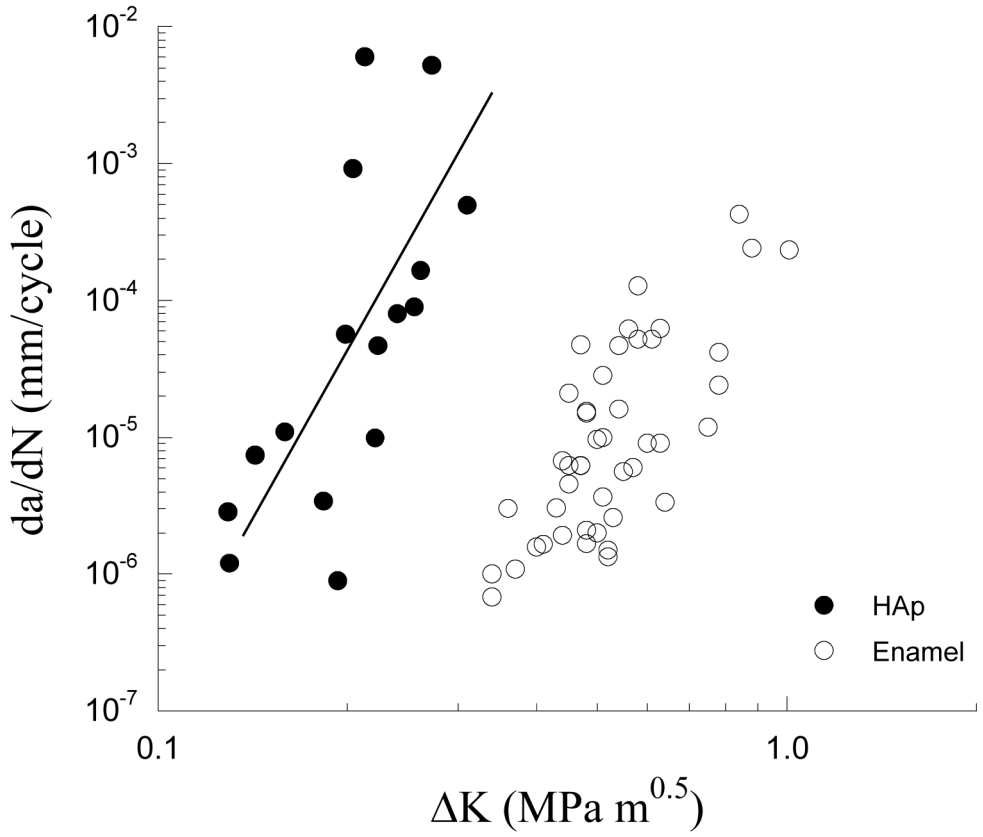

Figure 3.
Fatigue crack growth responses for the human enamel and sintered hydroxyapatite (HAp).

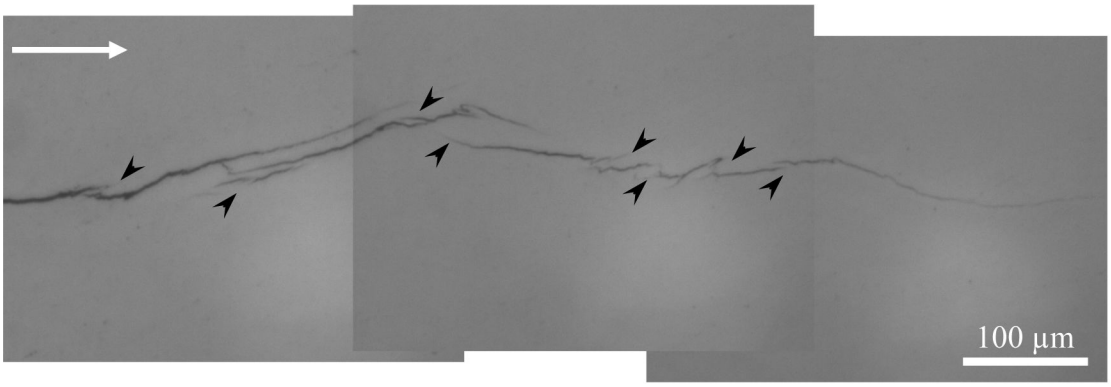

(a)

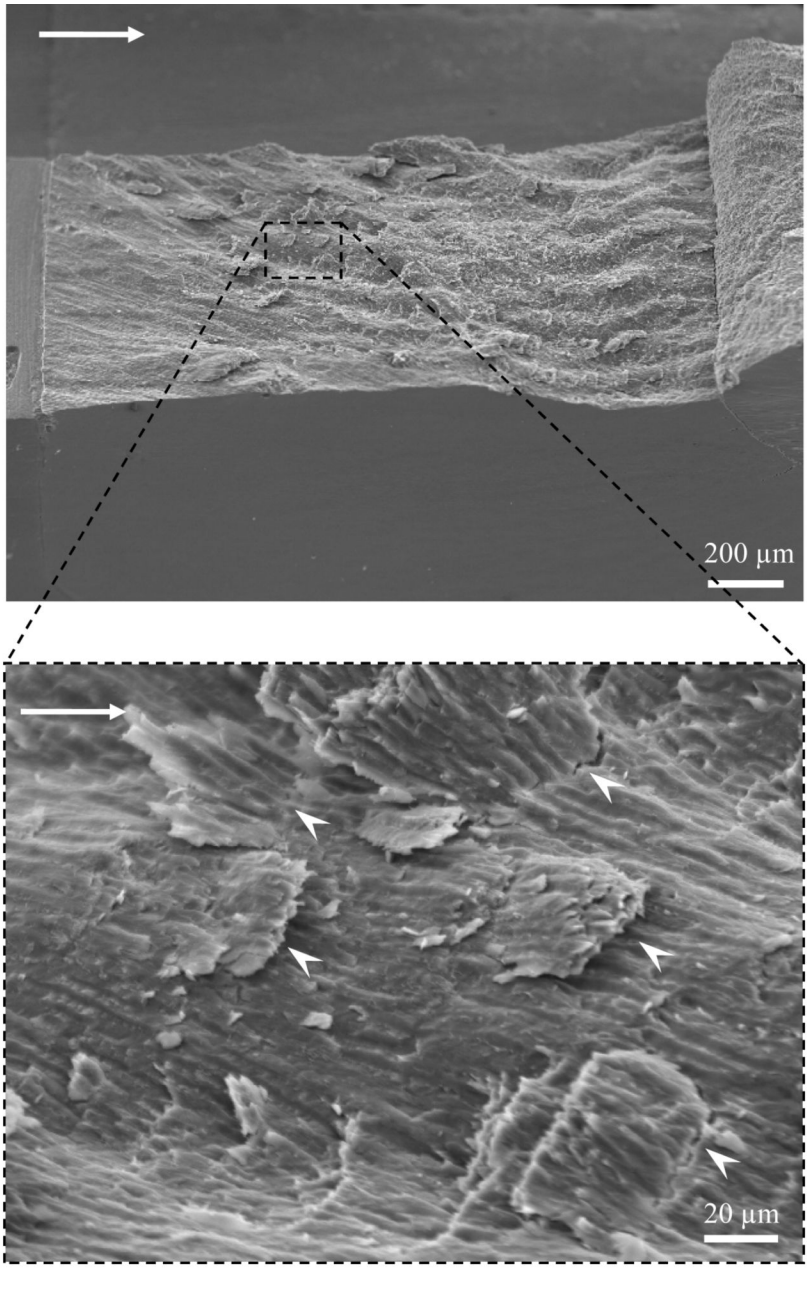

(b)

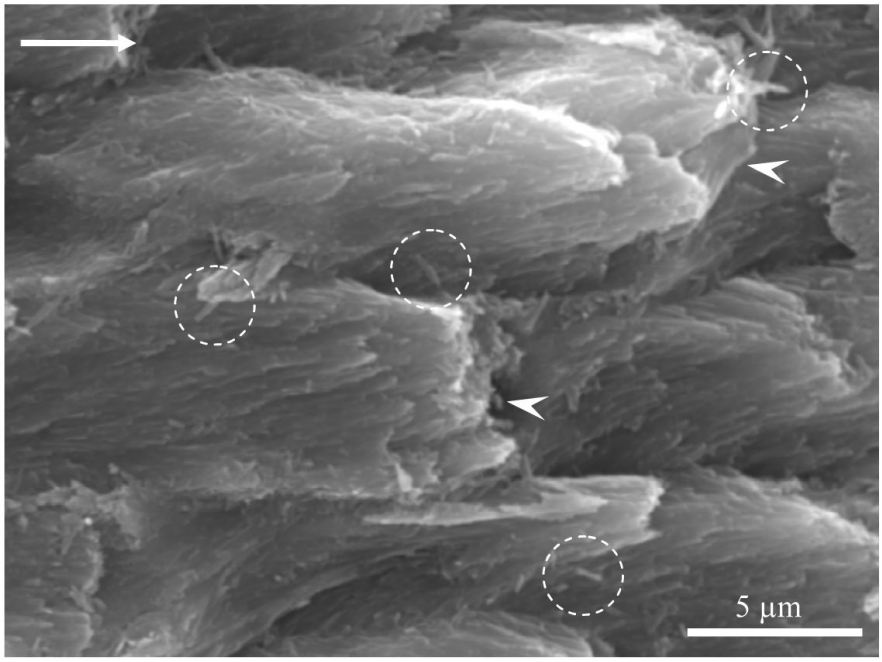

(d)

Figure 4.

Observations of crack extension in enamel.

(a) an optical micrograph of crack extension in enamel. Cyclic crack growth resulted in the formation of several unbroken ligaments of tissue that bridge the crack (black arrowheads). The direction of crack growth is from left to right

(b) variation in the fracture plane across the specimen thickness. Notice the larger amplitude and frequency of the waviness towards the inner enamel. Such features are formed due to crossing of bundles of prisms (also known as decussation). Notice the presence of a small portion of dentin and the DEJ at the end of the inset (the data reported in the study does not include the response where the crack reaches the DEJ as the crack becomes unstable prior to reaching the end of the inset)

(c) a view of smaller broken ligaments (white arrowheads) spread across the specimen thickness from (b). The image was taken at the surface corresponding to steady state growth ($\Delta K \sim 0.6$ MPa·$m^{0.5}$)

(d) crack extension in decussated enamel and fracture of individual prisms (indicated by white arrowheads). Note the individual and small groups of nano crystalline rods that also served as ligaments in the fracture process (circled region)

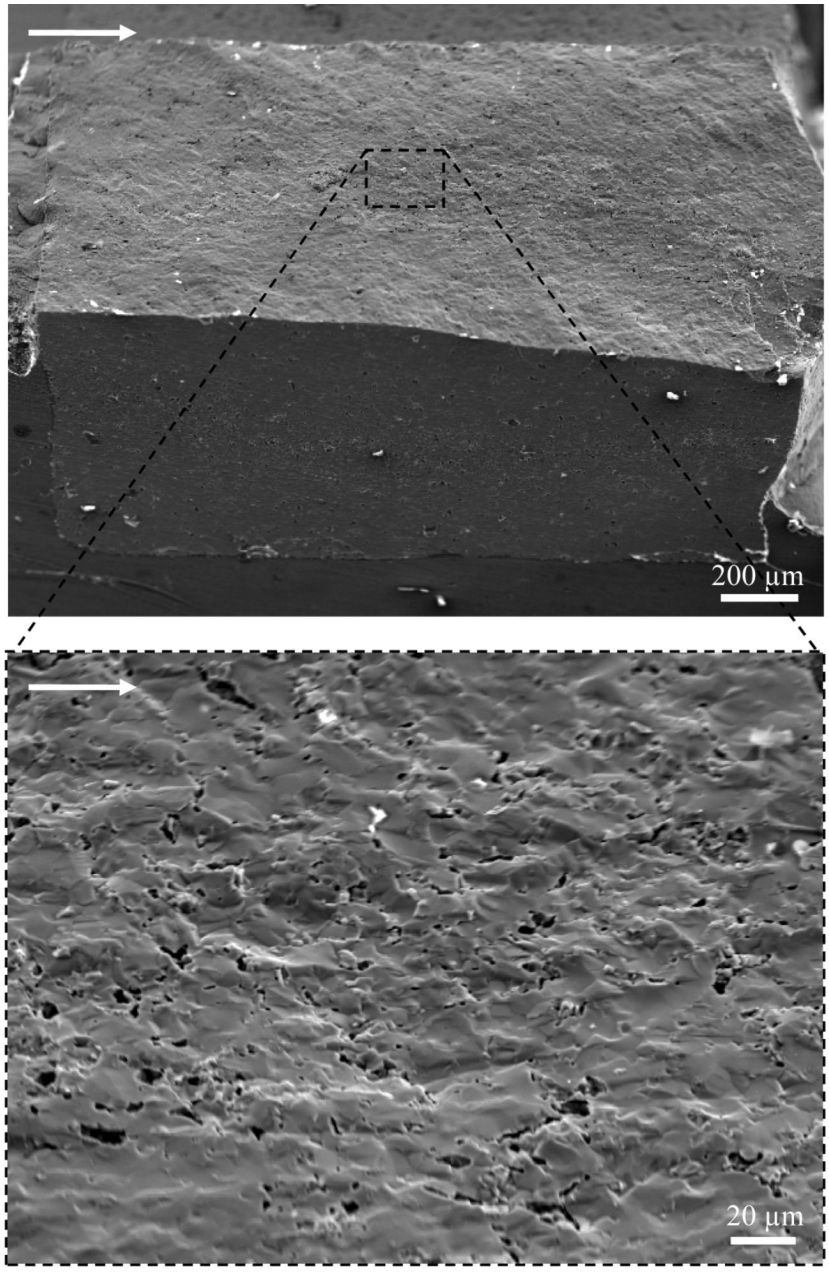

(a)

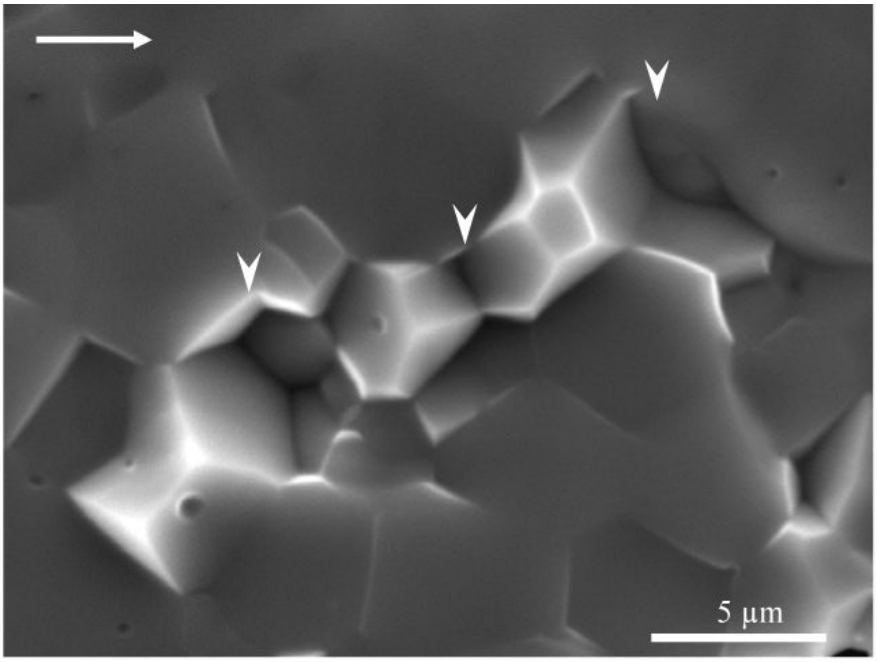

(c)

Figure 5.
Observations of crack extension in HAp.
(a) relatively smooth fracture plane of HAp compared to enamel in Figure 4
(b) a magnified view of fracture plane showing voids across the specimen thickness. The image was taken at the surface corresponding to steady state growth ($\Delta K \sim$ 0.2 MPa·$m^{0.5}$).
(c) A typical high magnification image of fracture surface of the sintered HAp. Notice the surface is primarily uniform but does exhibit a few HAp crystals (white arrowheads) pullout.

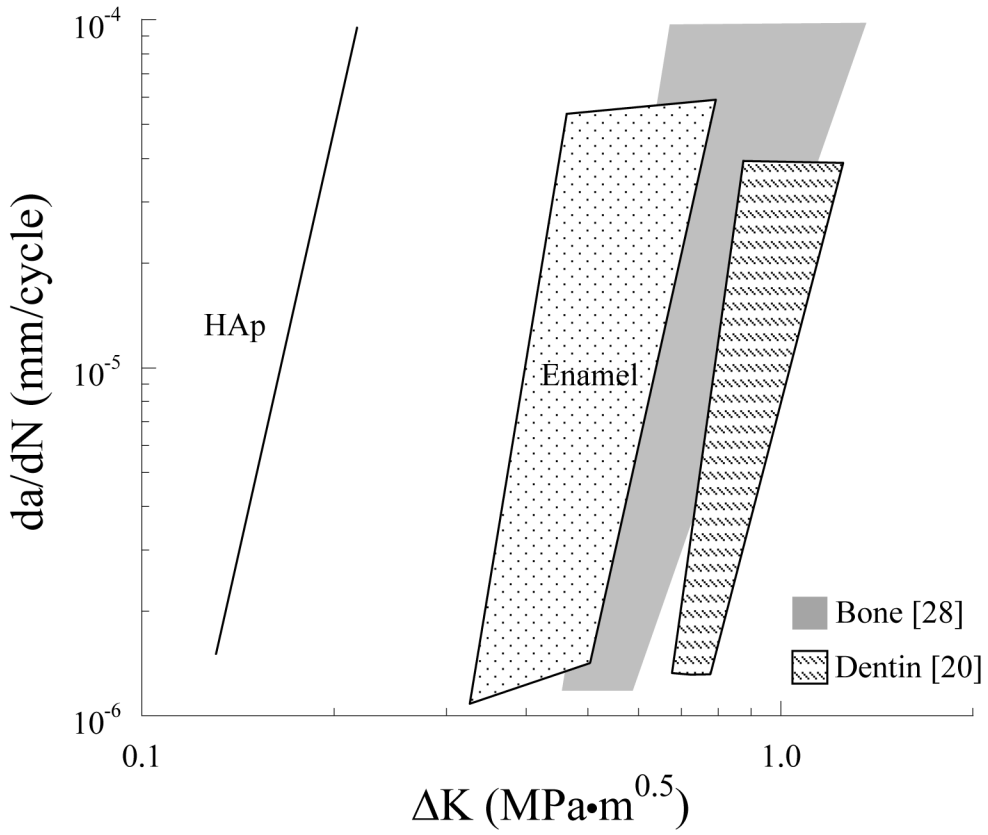

(a)

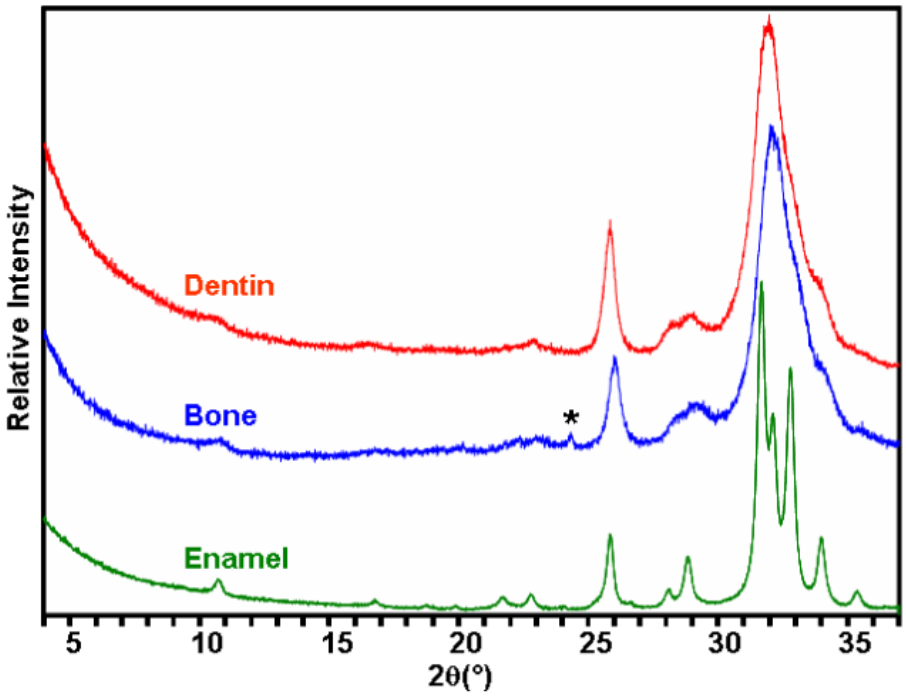

b)

Figure 6.

Comparison of fatigue crack growth response and chemistry of enamel with bone and dentin. (a) the data in Figure 3 are compared with results from fatigue crack growth in human dentin [20] (R=0.1, frequency 5 Hz) and human cortical bone [28] (R=0.1, frequency 1 Hz)
b) XRD patterns of enamel, bovine bone and dentin. * This small reflection comes from the aluminum holder

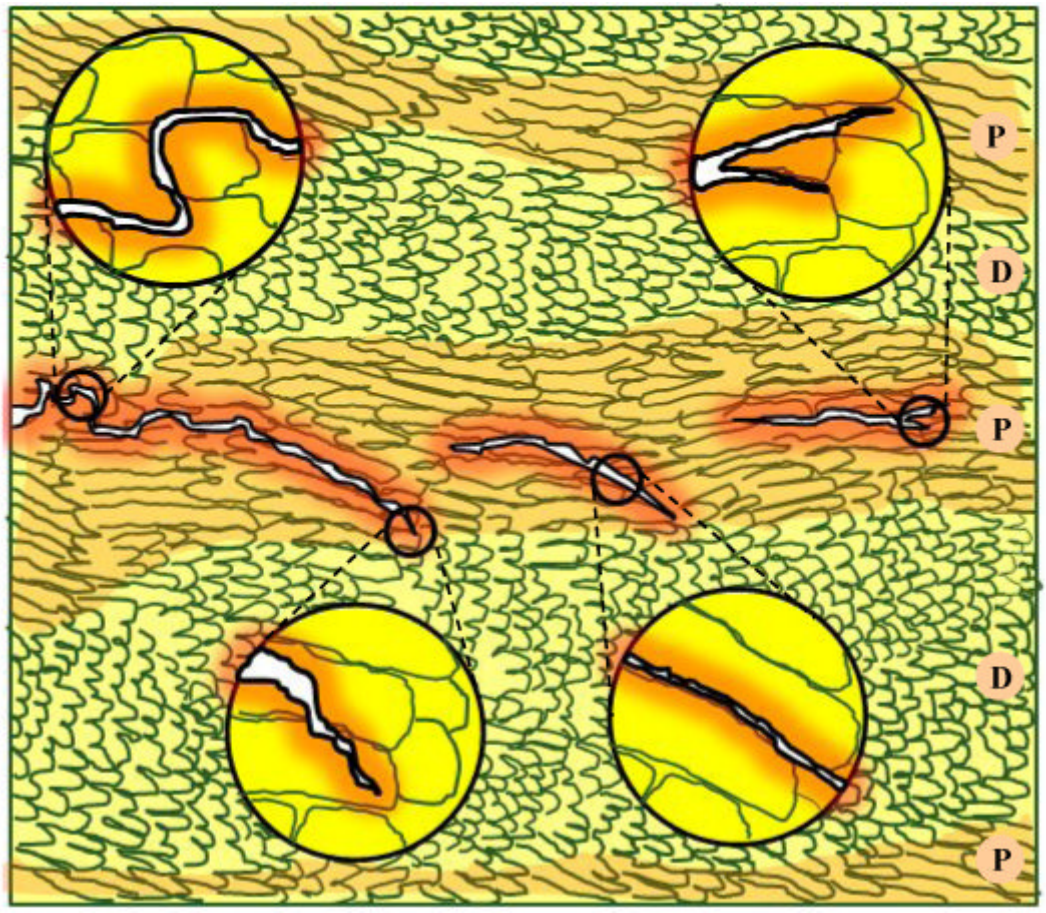

Figure 7.
A schematic description of crack growth through a decussated zone in enamel. Extension through prism decussation results in a highly tortuous path with multiple deflections. Arrest of cracks in enamel usually occurs while traversing from a less oblique prism orientation (indicated by the highlighted area), also known as the parazone (P) to a more oblique orientation, also known as the diazone (D). The crack traverses through a bundle of prisms along the interprismatic boundary and may undergo bifurcation in the search for a more energetically favorable path.

Table 1

Fatigue crack growth parameters for the enamel specimens

Number	Age/gender (years)	C (mm/cycle)·(MPa·m$^{0.5}$)$^{-m}$	m	R^2
1	27/F	3.5E-04	7.4	0.99
2	27/F	5.2E-04	8.3	0.93
3	17/M	2.4E-03	7.0	0.98
4	18/F	1.2E-04	8.0	0.99
5	18/F	2.9E-03	8.0	0.94
6	18F	5.0E-03	7.7	0.77
7	24/M	5.8E-05	5.6	0.99
8	22/F	6.3E-03	9.2	0.99
Average	21	8.7E-04	7.7 (1.0)	
Pooled		1.0E-04	3.9	0.38

specimens from the same molar.

Table 2

Fatigue crack growth parameters for the HAp specimens

Number	C (mm/cycle)·(MPa·m$^{0.5}$)$^{-m}$	m	R^2
1	1.7E+01	5.7	0.83
2	1.2E+00	6.4	0.99
3	1.3E+03#	11.9	0.99
4	1.6E+00	8.1	0.92
5	2.4E+00	7.4	1.00
6	2.7E+00	9.7	1.00
Average	2.0E+00	7.9 (1.4)	
Pooled	9.0E+00	7.6	0.42

represents an outlier which was not included inthe mean and standard deviation.